

Spurious Modes in Finite-Element Methods

Din Sun¹, John Manges², Xingchao Yuan¹,
Zoltan Cendes²

¹Ansoft Corporation
Four Station Square, Suite 600
Pittsburgh, PA 15219
Tel: (412) 261-3200
Fax: (412) 471-9427

²Department of Electrical and Computer Engineering
Carnegie Mellon University
Pittsburgh, PA 15213
Tel: (412) 268-2454
Fax: (412) 268-2860

1. Abstract

This paper describes the problem of spurious modes that appear with finite-element solutions of the vector wave equation. It explains that this problem is caused by inconsistent approximations of the static solutions to the wave equation. Tangential-vector finite elements are described that enforce the tangential continuity of the vector field, but leave the normal component discontinuous. It is shown that tangential elements provide consistent approximations of the static solutions to wave problems, and that spurious modes are not produced by this type of finite element. Applications of the theory presented include problems from microwave and antenna design, and from electromagnetic compatibility.

2. Introduction

The issue of spurious modes that arise with finite-element methods continues to provide a source of confusion in the electromagnetics community. Spurious modes are numerical solutions of the vector wave equation that have no correspondence to physical reality: these solutions are simply wrong answers, and should not be confused with experimental spurious modes that are unwanted-but-obviously-physically-existing modes. Another name sometimes used for numerical spurious modes is "vector parasites."

Early thinking about spurious modes attributed this problem to a deficiency in imposing the solenoidal nature of the field in the approximation process. A series of papers, beginning with Konrad [1] and followed by [2-4], expounded this idea. As a result, many researchers have been influenced by the notion that spurious modes are caused by the nonsolenoidal nature of finite-element-approximation procedures. Even the recently published and otherwise-excellent compendium by Silvester and Pelosi, on *Finite Elements for Wave Problems*, states: "To obtain a satisfactory general solution of the spurious mode problem, the magnetic and electric flux density vectors **B** and **D** must be constrained to be truly solenoidal" [5, p.83].

Yet, a body of literature now exists to show that the early thinking about the cause of spurious modes in finite-element methods is wrong. The true cause of spurious modes is the incorrect approximation of the null space of the curl operator. This result is shown in references [6-15]. Quoting from [7], "Provided the finite-element trial functions are able to approximate the nullspace of the

curl operator correctly, the eigenvalue $k=0$ will be computed exactly and it is only necessary to ignore these zero solutions." Indeed, high-order vector finite elements are now available that are not solenoidal, and yet do not exhibit spurious modes [11-15].

This paper examines the nature of spurious modes in finite-element methods, explains their origins, and describes their resolution. Our purpose is to clarify the issues by examining the literature on spurious modes, with reference to the two currents of thought described above. We will derive, in a simple way, the special forms that are required for vector elements to avoid spurious modes, and show the relationship between vector elements and the domain, range, and null space of the curl operator.

3. Vector wave equation

Finite elements were introduced in electrical engineering by Silvester, in 1969 [16]. He showed that the finite-element method had several advantages in solving homogeneous-waveguide problems, including geometric flexibility, derived by using triangles as the basic element shape, and high accuracy, derived by using a combination of high-order-approximation functions and variational principles.

Twenty-six years ago, it appeared, with the publication of Silvester's paper, that finite elements would soon become a common solution procedure in electromagnetics. Yet, decades would elapse after this early success before the finite-element method was applied correctly in other areas of high-frequency electromagnetics. The first attempts to extend the procedure beyond homogeneous waveguides failed. Solution of inhomogeneous-waveguide problems, either by using an $E_z - H_z$ formulation, or by using a three-component **E**- or **H**-field formulation, resulted in spurious modes [17-19]. The same phenomena occurred in attempts to solve three-dimensional problems. A survey of this early work appears in [5].

To understand the true cause of the difficulty, consider the vector wave equation, obtained by combining the two Maxwell curl equations:

$$\nabla \times \frac{1}{\mu_r} \nabla \times \mathbf{E} = k_0^2 \epsilon_r \mathbf{E}. \quad (1)$$

Here, **E** is the electric field, μ_r is the relative permeability, ϵ_r is

the relative permittivity, and $k_0^2 = \omega^2 \mu_0 \epsilon_0$. A similar equation, and a parallel treatment to the following, are possible in terms of \mathbf{H} . Solutions of Equation (1) must either be static, or be associated with a solenoidal flux, \mathbf{D} . To see this, take the divergence of both sides of Equation (1). Since the divergence of the curl of any vector is zero, it follows that

$$k_0^2 \nabla \cdot \epsilon_r \mathbf{E} = 0. \quad (2)$$

Hence, either $k_0 = 0$, which implies that $\omega = 0$, or $\nabla \cdot \mathbf{D} = 0$, where \mathbf{D} is the flux, $\mathbf{D} = \epsilon_0 \epsilon_r \mathbf{E}$.

Equation (1) was first solved using the finite-element method by Konrad [1], who was also the first to describe the problem of spurious modes arising from this equation. Konrad speculated, in his PhD thesis, that spurious modes are caused by solving Equation (1) alone, without explicitly enforcing the solenoidal nature of the flux [19]. Other researchers took his comments to heart, and attempted to find methods for imposing the nondivergence of flux in the finite-element method [2-4]. However, the above argument shows that this is not necessary: solutions of Equation (1) are either static, or have a solenoidal flux. The zero divergence of the flux is built into Equation (1) for all but static solutions.

Since the zero divergence of the flux is contained in Equation (1) for all but static solutions, we must look to the dc or static solutions of Equation (2) for the source of spurious modes. Associated with these static solutions is a potential function, ϕ , satisfying the equation

$$\mathbf{E} = -\nabla \phi. \quad (3)$$

Static electric fields form the null space of the curl operator, since $\nabla \times \mathbf{E} = \nabla \times \nabla \phi = 0$. Substituting Equation (3) into Equation (1) shows that electric fields derived from Equation (3) are eigenvectors of the vector wave equation, with eigenvalue zero:

$$\nabla \times \frac{1}{\mu_r} \nabla \times \nabla \phi = 0 = k_0^2 \epsilon_r \nabla \phi. \quad (4)$$

If we attempt to approximate the electric-field vector, \mathbf{E} , using ordinary scalar finite elements, as was done in [19], then it is impossible, in general, to find a scalar potential, ϕ , that satisfies Equation (3). To understand this relationship, consider the patch of elements shown in Figure 1. Let $\{\eta_i(x, y), i = 1, \dots, N\}$ represent the set of N linearly independent scalar first-order finite-element basis functions, defined for each node in a mesh of N nodes. Figure 1 shows this function for node 1. Note that this function is non-zero only in the elements around node 1: this region is called the support of $\eta_1(x, y)$. We can approximate the scalar potential, ϕ , in the meshed region, Ω , by the weighted sum

$$\phi(x, y) = \sum_{i=1}^N \phi_i \eta_i(x, y). \quad (5)$$

If we approximate each of the three Cartesian components of \mathbf{E} —namely E_x , E_y , and E_z , with the approximation in Equation (5), then each component of \mathbf{E} is continuous, but its derivative is not necessarily continuous. This is called C^0 continuity by mathematicians. Even though we never need to compute it, Equation (3) states that a scalar potential, ϕ , exists such that its negative gradient equals the electric-field vector. For this to be possible in this

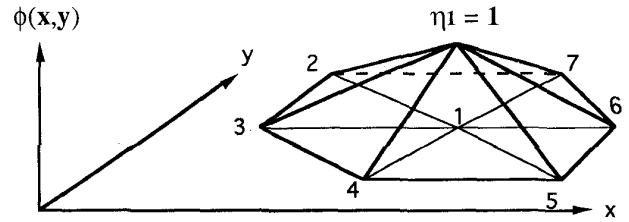


Figure 1. A patch of triangles in the $x-y$ plane, showing the faceted surface generated by the function $\eta_1(x, y)$ associated with node 1.

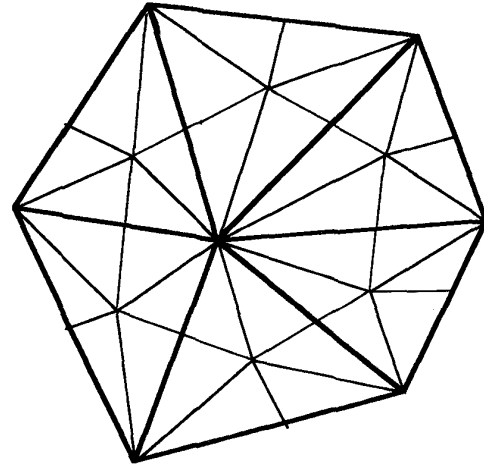


Figure 2. Each triangle in an arbitrary triangular mesh must be divided into six, to guarantee derivative continuity of the associated quadratic surface.

case, ϕ must be a quadratic, and it must have continuous x , y , and z derivatives, called C^1 continuity. However, reference [20] shows that quadratic C^1 piecewise polynomials do not exist over an arbitrary mesh. Quadratic C^1 piecewise polynomials are possible only over special meshes.

As explained in [20], quadratic C^1 meshes are formed by subdividing each of the triangles in an arbitrary triangular mesh into six triangles, as shown in Figure 2. On such subdivided meshes, it is possible to define a quadratic scalar potential having a first-order gradient. Consequently, on such special meshes, the null space of the curl operator is approximated correctly, and all $k = 0$ eigenvalues are computed as exactly zero. On arbitrary meshes, the approximation of the null space is very poor, and the zero eigenvalues are approximated by large numbers. The eigenvectors corresponding to these poorly approximated null vectors form the spurious modes which occur in finite-element analysis. It is demonstrated in [8] that tweaking the positions of some of the nodes in the C^1 mesh breaks the C^1 property, and introduces spurious modes, one spurious mode for each point moved. In fact, if one moves all of the nodes so that no zero eigenvalues remain, [8] shows that the number of spurious modes equals the dimension of the gradient of a scalar.

As an aside, it is interesting to note that early workers, who combined the finite-element method with the boundary-element

method to solve scattering problems, did not, at first, notice the spurious solutions [21-23]. This is because they looked, at first, at the far-field solution, which was correct. It was only after they examined the near-field solution that they noticed that something was drastically wrong. How could completely wrong near-field solutions produce correct far-field solutions? The explanation is that spurious modes are badly formed static solutions, and static solutions don't radiate. The far field, computed from a hybrid finite-element-boundary-element method, is correct even if spurious modes are present, because only the nonstatic components of this solution provide nontrivial far-field values.

4. Tangential vector finite elements

Since ordinary node-based finite elements require the use of special meshes to avoid the occurrence of spurious modes, the question arises, Is it possible to define new types of approximation functions that avoid spurious modes altogether? To answer this question, consider what happens to \mathbf{E} if ϕ is approximated by the first-order finite elements in Figure 1. Since the finite-element approximation is continuous along the element edges, the derivative tangent to each element edge will be continuous. However, the normal derivative along each edge will be discontinuous, since the finite-element approximation has a crease there. Consequently, if ϕ is to be approximated by first-order finite elements, the approximation for \mathbf{E} must be such that its tangential components are continuous, but its normal components are discontinuous.

Now, consider the element defined in Figure 3a. While the following presentation is two-dimensional, similar results hold in three dimensions. First, define the variables $\{e_i = \ell_i E_i, i = 1, 2, 3\}$, where E_i is the component of the electric field tangent to element edge i , and ℓ_i is the length of edge i . Let the electric field be approximated as

$$\mathbf{E} = \sum_{i=1}^3 e_i \gamma_i(x, y), \quad (6)$$

where the $\gamma_i(x, y)$ represent vector-basis functions. Our task is to determine the functions $\gamma_i(x, y)$.

To proceed, we need to be able to evaluate the components of a vector tangent to the element edges. For this purpose, define ζ_i to be the homogeneous coordinate to vertex i , and $\hat{\mathbf{t}}_i$ and $\hat{\mathbf{n}}_i$ to be unit vectors tangent and normal, respectively, to the side opposite vertex i , as in Figure 3b. Simple geometry shows that the dot product of the unit vectors is given by

$$\hat{\mathbf{T}} \cdot \hat{\mathbf{N}}^T = -\Delta L^{-1} S L^{-1}, \quad (7)$$

where Δ is plus-or-minus twice the triangle area, and

$$\hat{\mathbf{T}} = \begin{bmatrix} \hat{\mathbf{t}}_1 \\ \hat{\mathbf{t}}_2 \\ \hat{\mathbf{t}}_3 \end{bmatrix}, \quad \hat{\mathbf{N}} = \begin{bmatrix} \hat{\mathbf{n}}_1 \\ \hat{\mathbf{n}}_2 \\ \hat{\mathbf{n}}_3 \end{bmatrix}, \quad L = \begin{bmatrix} \ell_1 & 0 & 0 \\ 0 & \ell_2 & 0 \\ 0 & 0 & \ell_3 \end{bmatrix}, \quad S = \begin{bmatrix} 0 & -1 & 1 \\ 1 & 0 & -1 \\ -1 & 1 & 0 \end{bmatrix}. \quad (8)$$

Following [15], we write the electric field in terms of the three normal unit vectors

$$\mathbf{E}(x, y) = \hat{\mathbf{N}} E^{(N)}(\zeta_1, \zeta_2, \zeta_3). \quad (9)$$

Here $E^{(N)}(\zeta_1, \zeta_2, \zeta_3)$ are three components of the electric field in the three directions $\hat{\mathbf{n}}_i$. Note that these three components are not unique, since $\mathbf{E}(x, y)$ is a two-component vector.

Now, we expand $E^{(N)}$ in terms of as-yet-unknown polynomials $\gamma_{ij}(\zeta_1, \zeta_2, \zeta_3)$. Since there are three rows in Equation (9) and three coefficients e_i , we write these polynomials as a 3×3 matrix $\Gamma(\zeta_1, \zeta_2, \zeta_3)$. The result is

$$E^{(N)} = \frac{1}{\Delta} L \Gamma(\zeta_1, \zeta_2, \zeta_3) \underline{e}, \quad (10)$$

where

$$\Gamma = \begin{bmatrix} \gamma_{11} & \gamma_{12} & \gamma_{13} \\ \gamma_{21} & \gamma_{22} & \gamma_{23} \\ \gamma_{31} & \gamma_{32} & \gamma_{33} \end{bmatrix}, \quad \underline{e} = \begin{bmatrix} e_1 \\ e_2 \\ e_3 \end{bmatrix}. \quad (11)$$

The tangential components of \mathbf{E} are

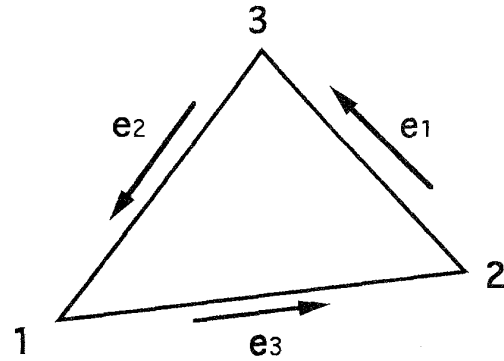


Figure 3a. The zeroth-order tangential-vector finite element.

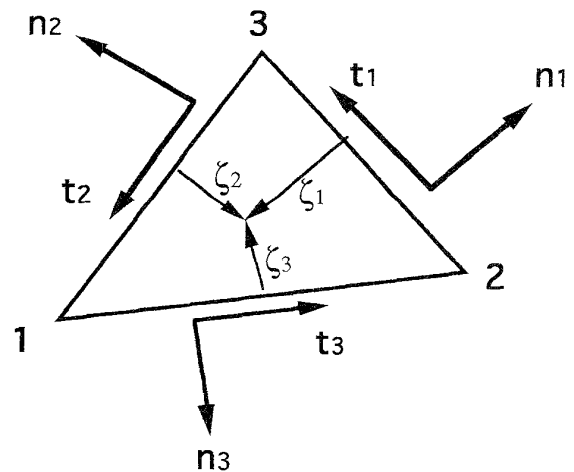


Figure 3b. Definitions of the unit-tangent and unit-normal vectors, and of the homogeneous coordinates ζ_i .

$$\begin{aligned}\hat{\mathbf{T}} \cdot \mathbf{E}(x, y) &= \hat{\mathbf{T}} \cdot \hat{\mathbf{N}} E^{(N)} \\ &= -L^{-1} S \Gamma(\zeta_1, \zeta_2, \zeta_3) \underline{\xi}.\end{aligned}\quad (12)$$

On side 1, where $\zeta_1 = 0$, we want $L \hat{\mathbf{T}} \cdot \mathbf{E} = e_1$. Similarly, on side 2, where $\zeta_2 = 0$, we want $L \hat{\mathbf{T}} \cdot \mathbf{E} = e_2$, and on side 3, where $\zeta_3 = 0$, we want $L \hat{\mathbf{T}} \cdot \mathbf{E} = e_3$. The top, center, and bottom rows of Equation (12) thus imply

$$\begin{aligned}\gamma_{31} - \gamma_{21} &= 1, & \gamma_{32} - \gamma_{22} &= 0, & \gamma_{33} - \gamma_{23} &= 0 \\ \gamma_{11} - \gamma_{31} &= 0, & \gamma_{12} - \gamma_{32} &= 1, & \gamma_{13} - \gamma_{33} &= 0. \\ \gamma_{21} - \gamma_{11} &= 0, & \gamma_{22} - \gamma_{12} &= 0, & \gamma_{23} - \gamma_{13} &= 1\end{aligned}\quad (13)$$

A possible solution of Equation (13) is

$$\Gamma = \begin{bmatrix} 0 & \zeta_3 & -\zeta_2 \\ -\zeta_3 & 0 & \zeta_1 \\ \zeta_2 & -\zeta_1 & 0 \end{bmatrix}.\quad (14)$$

Combining Equations (9), (10), and (14) provides

$$\mathbf{E} = [(\hat{\mathbf{n}}_2 \ell_2 \zeta_3 - \hat{\mathbf{n}}_3 \ell_3 \zeta_2) (\hat{\mathbf{n}}_3 \ell_3 \zeta_1 - \hat{\mathbf{n}}_1 \ell_1 \zeta_3) (\hat{\mathbf{n}}_1 \ell_1 \zeta_2 - \hat{\mathbf{n}}_2 \ell_2 \zeta_1)] \quad (15)$$

Finally, note that the gradient of the homogeneous coordinate ζ_i is simply

$$\nabla \zeta_i = -\frac{\hat{\mathbf{n}}_i}{h_i}, \quad (16)$$

where h_ℓ is the altitude of vertex ℓ . Since $\Delta = \ell_i h_i$, for $\gamma_i(x, y)$ of Equation (6) we obtain the simple form

$$\gamma_i(x, y) = \zeta_j \nabla \zeta_k - \zeta_k \nabla \zeta_j. \quad (17)$$

Here, the subscripts (i, j, k) are cyclic modulo three.

Setting the coefficients e_i to be the same in adjacent finite elements imposes tangential continuity of the vector field without imposing normal continuity. Since the gradient of first-order finite elements has tangential, but not normal, continuity, the scalar defining the null space of the curl operator, using the approximation of Equation (8), is the set of C^0 continuous polynomials, i.e., first-order finite elements. The fact that first-order scalar elements and the polynomials $\gamma_i(x, y)$ form a consistent electric-field scalar-potential pair, over an arbitrary mesh of elements, implies that the null space of the curl operator is properly modeled, and that no spurious modes are produced.

The approximation functions in Equations (8) and (9) are often called edge elements. Notice, however, that they are actually just the tangential counterpart to the Rao-Glisson-Wilton element, and other higher-order elements that impose normal instead of tangential continuity [24, 25]. For this reason, we will refer to the element in Figure 3a as a tangential-vector element, and to the Rao-Glisson-Wilton element as a normal-vector element. This designation is also more appropriate with high-order vector elements, where some variables are associated with faces and with volumes rather than with edges. Indeed, Bossavit shows that tangential-vector finite elements are just one of several manifestations of Whitney forms in electromagnetics [26]. If one approximates a

scalar by piecewise C^0 polynomials, then the electric field must be approximated by vectors that have tangential, but not normal, continuity. The first of these quantities is called a zero-form, and the second is called a one-form. Currents and fluxes must be represented by two-forms that have normal, but not tangential, continuity. Lastly, the divergence of currents and fluxes are discontinuous scalars that are called three-forms.

Although the vector polynomials $\gamma_i(x, y)$ are solenoidal inside the elements, the global approximation is not solenoidal. The global approximation resulting from Equation (6) actually includes a nonzero divergence along the edges. The success of zeroth-order edge elements in eliminating spurious modes is due to their relationship to the null space, and not to their solenoidal nature.

Since the normal component of the electric field is not specified by Equation (6), how is the normal component specified in the solution process? After all, physical fields exhibit normal flux continuity. How is this property imposed? The answer to this question is that normal-flux continuity is a natural boundary condition, in the variational process used to set up the finite-element equations. This result is proved in [14, 15]. Continuity of the normal-flux component is satisfied in a least-squares sense in vector problems, analogous to normal-derivative continuity with scalar problems.

5. Trees and cotrees

References [27-30] provide some fascinating relationships between edge elements and graph theory. To understand these relationships, consider a finite-element mesh, containing T triangles covering a region Ω , as indicated in Figure 4. Let us define the edge-element space E as the set of all fields \mathbf{E} formed by taking a linear combination of the edge-element basis functions associated with all of the edges of this mesh:

$$E = \left\{ \mathbf{E} \mid \mathbf{E} = \sum_{i=1}^M e_i \gamma_i(x, y) \right\}, \quad (18)$$

where M indicates the number of edges in the mesh.

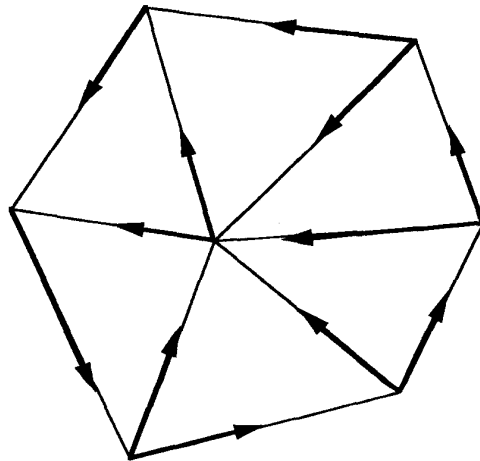


Figure 4. The edge-element space E , defined over a patch of elements. Here, $T = 6$, $N = 7$, and $M = 12$.

Two subspaces of E are important in understanding its structure. From the earlier discussion, we need to separate E into fields that have zero curl and those that do not. Let us denote the curl null space by the symbol G , and write

$$G = \{ \mathbf{E} | \mathbf{E} \in E \text{ and } \nabla \times \mathbf{E} = 0 \text{ in } \Omega \}. \quad (19)$$

To construct the second subspace of E we first need to define the "tree" of a finite-element mesh. This is defined as any set of edges connecting all nodes, but forming no closed loops. One possible tree for the mesh of Figure 4 is shown in Figure 5.

Now, define the cotree space, C , as the subspace of E with all edge variables on a tree set to zero:

$$C = \{ \mathbf{E} | \mathbf{E} \in E \text{ and } \mathbf{e}_i = 0 \text{ on a selected tree} \}. \quad (20)$$

The cotree subspace is different for each tree, but a tree always has $N-1$ branches, and so the dimension of C is always $\dim\{C\} = M - (N-1)$.

To determine the dimension of the space G , we note that $\nabla \times \mathbf{E} = 0 \Rightarrow \mathbf{E} = -\nabla\phi$. For the special function $\phi = 1$,

$$1 = \sum_{i=1}^N \eta_i(x, y). \quad (21)$$

Taking the gradient of this equation shows that the gradients of the functions $\eta_i(x, y)$ are not independent. In particular, we find that

$$0 = \sum_{i=1}^N \nabla \eta_i(x, y). \quad (22)$$

Any function other than $\phi = 1$ has a nonzero gradient. Thus, Equation (22) may be used to eliminate one of the vectors $\nabla \eta_i(x, y)$ in favor of the others, but then the rest are independent. It follows from this that G has dimension $\dim\{G\} = N-1$, and is identical to the gradient space

$$G = \left\{ \mathbf{E} | \mathbf{E} = \sum_{i=1}^{N-1} \phi_i \nabla \eta_i(x, y) \right\}. \quad (23)$$

It is interesting to note that the dimension of the gradient space for a connected mesh of elements is just one less than the dimension of the scalar space. The dimension of an individual first-order finite element is three, while its gradient is a constant vector specified by two parameters. Many dependencies exist, however, in the gradient of a mesh of connected elements, since tangential-field components must be continuous along internal edges. The above analysis shows that the consequence of these dependencies is to reduce the dimension from $2T$ to $N-1$.

The significance of C and G is explained in [28]. The line integral of \mathbf{E} around the three sides of a triangle is just

$$\int_{\Delta} \mathbf{E} \cdot d\mathbf{l} = e_1 + e_2 + e_3. \quad (24)$$

Since the curl of each $\gamma_i(x, y)$ is a constant, the only way to produce a zero curl in the cotree space C is to set $e_i = 0$ on all cotree

edges in the mesh. Thus, the only common element of the cotree space C , and of the curl null space G , is the null field $\mathbf{E} = 0$:

$$C \cap G = \{0\}. \quad (25)$$

Since $\dim\{C\} + \dim\{G\} = M = \dim\{E\}$, it follows that the cotree space and the curl space combine to form the entire edge space:

$$C \cup G = E. \quad (26)$$

Notice that although C and G separate E into two parts, the elements of C need not be orthogonal to the elements of G . Although

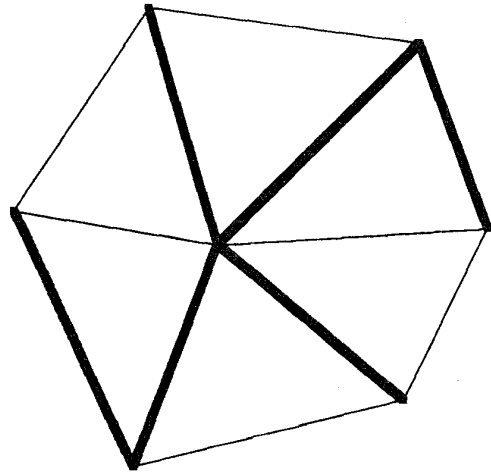


Figure 5. A tree of the graph of E . Here, $C = 6$.

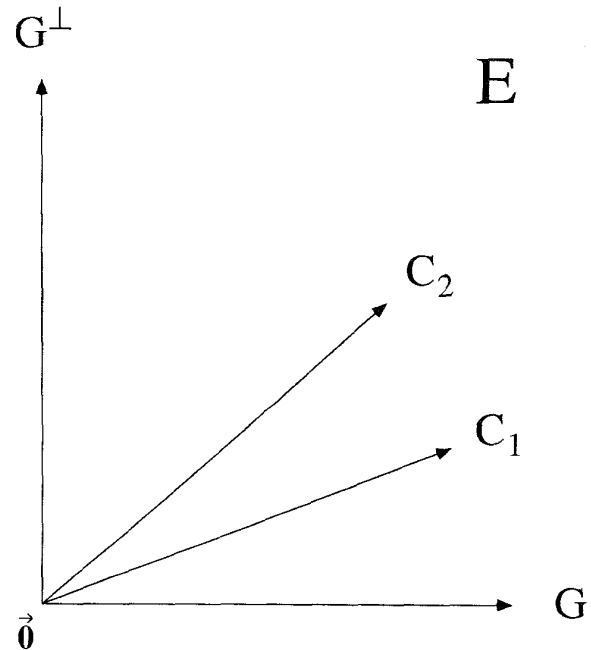


Figure 6. A pictorial representation of the decomposition of the edge space, E , into the cotree space, C_i , and the gradient space, G , using two different trees, $i=1$ and $i=2$.

the space G is not affected by the choice of the tree, different tree and cotree choices create many different spaces C_i in E . This relationship is represented symbolically as in Figure 6, where a two-dimensional plane represents the space E . The gradient space G is indicated by a horizontal vector, and its orthogonal complement, G^\perp , by a vertical vector. A particular choice of tree defines a cotree space C_1 , and is represented in Figure 6 by a linearly independent direction. Changing the tree provides a new direction C_2 . The two subspaces, C_i and G , span E for any choice of tree, and overlap only at the origin.

The decomposition in Equations (25) and (26) provides a natural partitioning of E for finite-element discretizations involving the curl operator. It is useful in gauging discretized potentials in quasistatic problems [27-29], and may be applied to the solution of the vector wave equation [32, 33]. For the sake of simplicity, consider solving the vector wave equation for the magnetic field, \mathbf{H} , instead of for the electric field, \mathbf{E} . Since $\dim\{G\} = N - 1$, we know that $N - 1$ zero-eigenvalue solutions will result in the vector wave equation, if \mathbf{H} is approximated by the edge-element space E . A similar result holds if \mathbf{E} is used instead of \mathbf{H} as the solution variable, although in this case, one must keep track of the number of tangential values set to zero on conducting surfaces. As explained in [33], these zero-eigenvalue solutions may be eliminated altogether by restricting the solution domain to lie in the orthogonal complement of G , indicated by the perpendicular vector G^\perp in Figure 6.

6. Higher-order elements

While the elements defined in Figure 3a work correctly, their rate of convergence is slow. This is because they approximate the tangential component of the electric field on each edge by a constant, and thus provide a zeroth-order rate of convergence. To achieve faster convergence, we must introduce higher-order polynomials in the approximation. One way to do this is to approximate the tangential component of the field along each edge by a p th-order polynomial. Since $p + 1$ points are required to define a p th-order polynomial, $p + 1$ nodes are used on each side. A polynomial with the required interpolation property is

$$\mathbf{E}_e(\mathbf{x}, y) = \sum_{i=1}^3 \left[\sum_{s=0}^{p-1} e_i^s \alpha_s(\zeta_j, \zeta_k) \nabla \zeta_k - e_i^p \alpha_p(\zeta_j, \zeta_k) \nabla \zeta_j \right], \quad (27)$$

where $\alpha_s(\zeta_j, \zeta_k)$ are Lagrange interpolation polynomials in one dimension, and (i, j, k) are cyclic variables. Computations show, however, that the rate of convergence of the elements defined by Equation (27) is not as high as expected. For example, the rate of convergence of the six-parameter tangential element that is linear on each side is the same as that of the three-parameter tangential element that is constant on each side. Increasing the order of approximation of the tangential components, by doubling the number of variables, does not increase the accuracy of the computation. Why?

The answer to this question comes from realizing that to achieve p th-order convergence, the approximation must contain all of the terms in a p th-order polynomial in the range space of the curl operator. The rate of convergence cannot be p th order if some of the p th-order terms are missing from the range space. However, the dimension of the complete linear space is not at all obvious: one must be careful not to include too many such terms, lest they fail to

meet the requirement of linear independence. Fortunately, the result was determined by Nedelec [34]. Unfortunately, Nedelec's derivation is difficult to follow; here, we present a simpler derivation.

To begin, note that a complete polynomial of order p contains

$$\dim\{\phi^p\} = (p+1)(p+2)/2 \quad (28)$$

terms. We keep track of the various terms in this derivation in Table 1. Complete polynomials are expressed here as standard scalar finite elements.

Now, consider the null space of the curl operator. This is of the form $\nabla\phi$, where ϕ is a complete polynomial of order $p+1$. According to Equation (23), the dimension of the gradient space, G^p , of a p th-order complete polynomial is

$$\dim\{G^p\} = \dim\{\phi^{p+1}\} - 1. \quad (29)$$

The curl of a two-dimensional, two-component field is a one-component vector directed perpendicular to the field. From Maxwell's equations, we can write

$$\nabla \times \mathbf{E} = -j\omega B_z \hat{\mathbf{z}}. \quad (30)$$

Our goal is to generate a vector polynomial that will yield a complete polynomial of order p when we take its curl. Let us define the space

$$R^p = \left\{ \mathbf{B} = \hat{\mathbf{z}} B_z^p(x, y) \mid B_z^p(x, y) \text{ is a complete polynomial of order } p \right\} \quad (31)$$

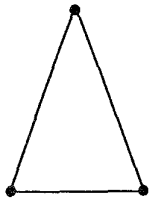

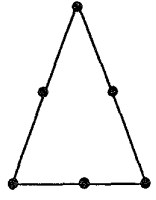
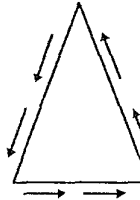
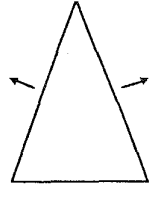
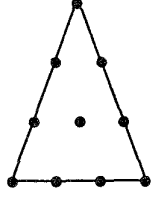
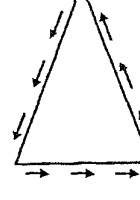
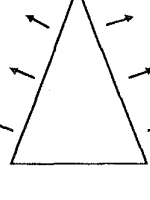
The dimension of R^p is given by Equation (28).

We need to generalize the edge space, E , of Equation (18). This generalization is called the $H^p(\text{curl})$ space in the literature. Here, p indicates the order of the complete polynomial in the range of the curl operator, and the lowest-order space, E , is designated as $H^0(\text{curl})$. The dimension of $H^p(\text{curl})$ is the sum of the dimensions of G^p and R^p :

$$\begin{aligned} \dim\{H^p(\text{curl})\} &= \dim\{G^p\} + \dim\{R^p\} \\ &= (p+1)(p+3) \end{aligned} \quad (32)$$

Now, consider the process of forming a p th-order tangential-vector finite element. To do so, we must first ensure that the tangential component is continuous along each side to p th order. One way to do this is to have the tangential component interpolate at $(p+1)$ points along each side, as provided in Equation (27). This is illustrated pictorially, for $p = 0, 1, 2$, in column six of Table 1. It follows that $p(p+1)$ additional variables must be added to the tangential-continuity variables in Equation (27) to ensure completeness of the $H^p(\text{curl})$ space. This is indicated in column seven of Table 1. Lastly, we need to add these variables in such a way that they won't disturb the tangential-continuity properties built into Equation (27). One logical way to do this is to add vector functions that interpolate to the normal components of the field on the element edges, as illustrated in the last column of Table 1.

Table 1. The dimension of the space $H^p(\text{curl})$.

order	scalar ϕ^{p+1}	$\dim\{G^p\}$ $\nabla\phi^{p+1}$	$\dim\{R^p\}$ for completeness	$\dim\{H^p(\text{curl})\}$ $= \dim\{G^p\} +$ $\dim\{R^p\}$	tangential interpolation	extra domain variables needed	added domain variables
p	$\frac{(p+2)(p+3)}{2}$	$\frac{(p+1)(p+4)}{2}$	$\frac{(p+1)(p+2)}{2}$	$(p+1)(p+3)$	$3(p+1)$	$p(p+1)$	
$p=0$		$3 - 1 = 2$	1	$2 + 1 = 3$		$3 - 3 = 0$	none
$p=1$		$6 - 1 = 5$	3	$5 + 3 = 8$		$8 - 6 = 2$	
$p=2$		$10 - 1 = 9$	6	$9 + 6 = 15$		$15 - 9 = 6$	

The first such elements were defined by Sun and Cendes who, for $p > 0$, added the functions \mathbf{E}_f to the functions \mathbf{E}_e in Equation (18) [11,14]:

$$\mathbf{E} = \mathbf{E}_e + \mathbf{E}_f, \quad (33)$$

where

$$\mathbf{E}_f = \zeta_1 \zeta_2 P^{(p-1)}(\zeta_1, \zeta_2) \nabla \zeta_3 + \zeta_2 \zeta_3 Q^{(p-1)}(\zeta_2, \zeta_3) \nabla \zeta_1. \quad (34)$$

Here, $P^{(p-1)}(\zeta_1, \zeta_2)$ and $Q^{(p-1)}(\zeta_1, \zeta_2)$ are polynomials of degree $(p-1)$ in two dimensions. It is important to note that while the functions \mathbf{E}_f are related to the normal components of the vector on the element faces, the normal component of the field is not interpolated by the full expansion of \mathbf{E} . This is in contrast to the edge-based functions \mathbf{E}_e that do interpolate to the tangential components of the field on the element edges. Extensions of Equations (24) and (25) to three dimensions is given in Appendix A.

The choice of polynomials defining tangential-vector finite elements is not unique [15]. The first-order complete $H^1(\text{curl})$ element contains eight independent variables, as indicated in Table 1. It is possible to define six normal functions \mathbf{E}_f , distributed with two to each of the three sides, as opposed to the three-functions-on-two-sides arrangement of Equation (34), indicated in

Table 1. A particularly good expression of this element is published in [12]. For the first-order $H^1(\text{curl})$ space, Peterson has recently proposed modifying the functions in [12] to make them more symmetric [13]. However, both sets of functions, those in [12] and those in [13], are complete to first order in the range space of the curl operator. One therefore expects them to provide identical results, except for round-off error. That this is indeed the case is demonstrated in Figure 7.

Notice that the p th-order complete tangential-vector finite elements are paired with the $(p+1)$ th-order scalar-finite elements. This is because the gradient of the $(p+1)$ th-order complete scalar-finite elements share the same function space as the p th-order complete-tangential elements. Thus, the null space of the curl operator is correctly modeled, and all $k=0$ eigenvalues are approximated as exactly zero, so that no spurious modes result. The only case in which the approximation functions are solenoidal inside the element is zeroth order. The divergence of all higher-order elements is, in general, nonzero everywhere.

Since the linear element in Table 1 lacks three-fold symmetry, one is tempted to introduce a third function on the empty side. However, this violates the analysis in Equations (28)-(32), and results in new spurious modes. In this case, one is attempting to use nine functions in the approximation, when only eight of them can be independent. The number of spurious modes generated equals the

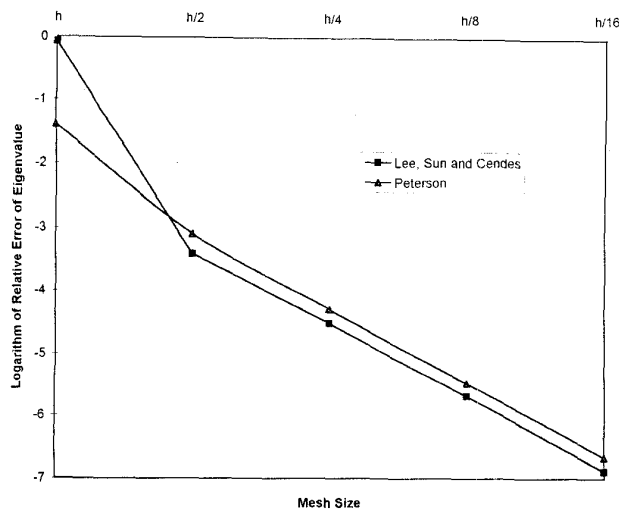


Figure 7. The convergence rate of the Lee-Sun-Cendes element, and of the Peterson element.

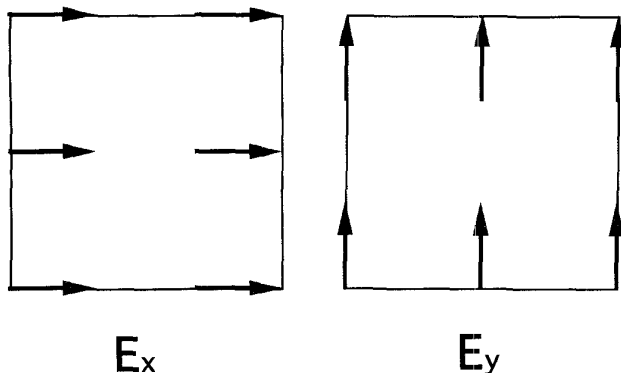


Figure 8. First-order covariant-projection elements.

number of elements, since there is one extra function in each element. Thus, while bad approximations of the null space of the curl operator can cause spurious modes, they are not the only cause. Even if the null space is correctly modeled, one must ensure that the approximating functions form a linearly independent set in the range space of the curl operator. Reference [15] separates spurious modes into two types. Type A spurious modes are the result of incorrect approximations of the null space of the curl operator, while Type B spurious modes are caused by using a linearly dependent set of vector-basis functions.

7. Covariant-projection elements

The above ideas apply to rectangular finite elements as well as to the triangular finite elements described above. The rectangular versions of tangential-vector elements are often called covariant-projection finite elements [9]. The lowest-order covariant-projection finite element was first described by Hano, who was the first to provide a consistent finite-element solution of the vector wave equation [6]. It is interesting to note that Hano's element employs exactly the same approximation function that is used in the Yee FDTD algorithm.

The Hano element is extended to higher order in [11, 14]. The argument is as follows. Let ϕ be approximated by the p th-order Cartesian product

$$\phi(x, y) = \sum_{i=1}^{p+1} \sum_{j=1}^{p+1} \phi_{ij} \alpha_i^{(p)}(x) \alpha_j^{(p)}(y), \quad (35)$$

where the $\{\alpha_i^{(p)}(x), i = 1, \dots, p+1\}$ are the set of p th-order Lagrange interpolation polynomials. Then, in order to make \mathbf{E} compatible with $\nabla\phi$, \mathbf{E} must take the form

$$\mathbf{E}(x, y) = \hat{\mathbf{x}} \sum_{i=1}^{p+1} \sum_{j=1}^{p+1} \mathbf{E}_{x_{ij}} \alpha_i^{(p-1)}(x) \alpha_j^{(p)}(y) + \hat{\mathbf{y}} \sum_{i=1}^{p+1} \sum_{j=1}^{p+1} \mathbf{E}_{y_{ij}} \alpha_i^{(p)}(x) \alpha_j^{(p-1)}(y) \quad (36)$$

Figure 8 illustrates this element for $p = 2$. Notice that the curl of \mathbf{E} is

$$\nabla \times \mathbf{E} = \hat{\mathbf{z}} \left\{ \sum_{i=1}^p \sum_{j=1}^{p+1} \mathbf{E}_{x_{ij}} \alpha_i^{(p-1)}(x) \frac{\partial \alpha_j^{(p)}(y)}{\partial y} + \mathbf{E}_{y_{ij}} \frac{\partial \alpha_j^{(p)}(x)}{\partial x} \alpha_i^{(p-1)}(y) \right\}. \quad (37)$$

Since the derivative of a p th-order polynomial is $(p-1)$ th order, each polynomial in Equation (28) is $(p-1)$ th order.

To make Cartesian-product elements useful with irregular geometries, one must apply an isoparametric transformation. This is done in [9].

8. Applications

High-order tangential-vector finite elements were first applied to the solution of microwave problems in the program the *High-Frequency Structure Simulator (HFSS)*, developed by Ansoft Corporation, and marketed by the Hewlett-Packard Corporation [35]. This program combines a solid modeling system with automatic adaptive-mesh generation [36, 37] to produce a push-button solution to field problems. These elements and these procedures are also used in the program *Maxwell Eminence*, developed and marketed by Ansoft [38]. Some researchers have also recently reported developing similar procedures, using zeroth-order elements [39-41].

Tangential elements are useful for solving a large variety of electromagnetic-field problems. Here we present five examples: a waveguide filter, a traveling-wave tube, a patch antenna, a sinuous antenna, and an automotive EMC problem. Figure 9a shows the geometry of a waveguide filter, containing four cylindrical inductive posts. This waveguide is excited from the left by the TE_{10} mode; the task is to compute the spectral response of the reflection and transmission coefficients for this filter, between 10.2 and 10.7 GHz.

To solve this problem, the geometry is first entered using the solid-modeling system. The software computes the waveguide modes at the input and output ports, using two-dimensional finite-element analysis [42]. These waveguide modes are used in the trans-finite-element method, to simultaneously compute the three-dimensional electromagnetic fields and the scattering parameters [43]. Asymptotic-waveform evaluation (AWE) is used to generate

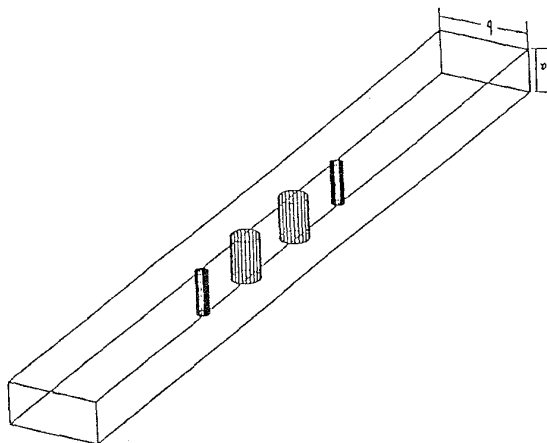


Figure 9a. A rectangular-waveguide filter with four inductive posts: $2a = b = 0.9$ inches.

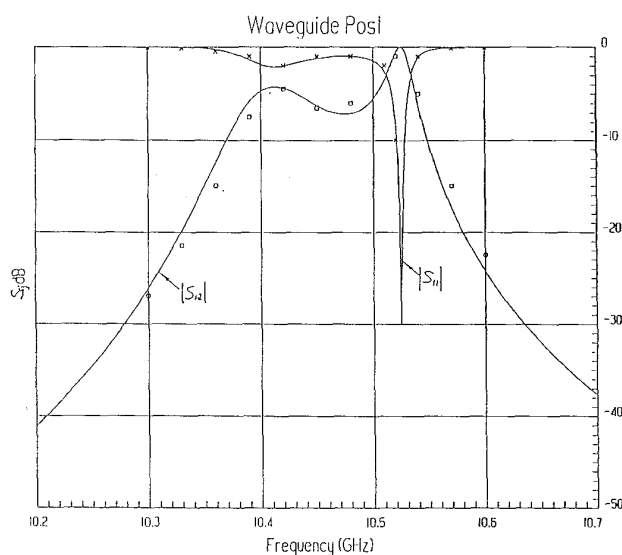


Figure 9b. A comparison of the predicted and measured s -parameters for the waveguide filter.

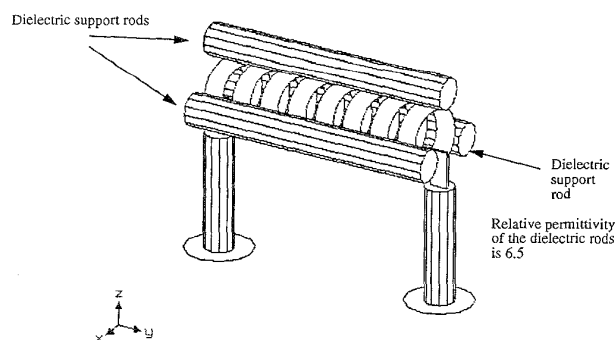


Figure 10a. A traveling-wave tube, consisting of an eight-turn helix and three dielectric supports.

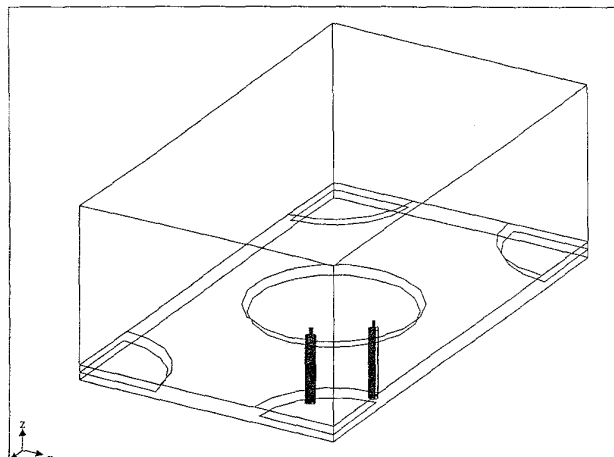


Figure 11a. One section of a phased-array patch antenna with coaxial feeds.

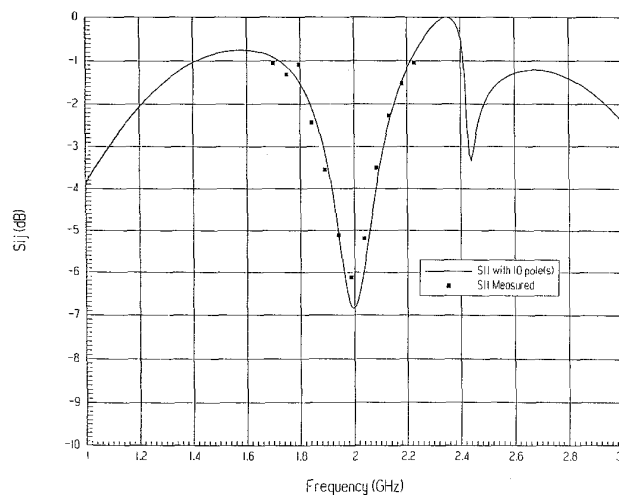


Figure 11b. A comparison of predicted and measured scattering parameters as a function of frequency.

Sinusoidal Antenna: Gain in (dB) vs. Theta, at 3000 MHz

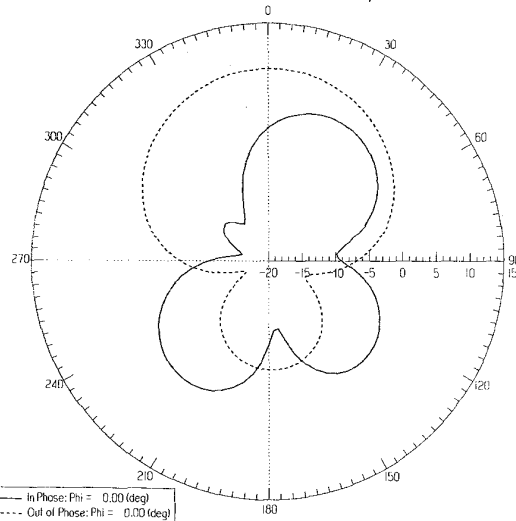


Figure 12b. The antenna gain versus theta for in-phase and out-of-phase excitations.

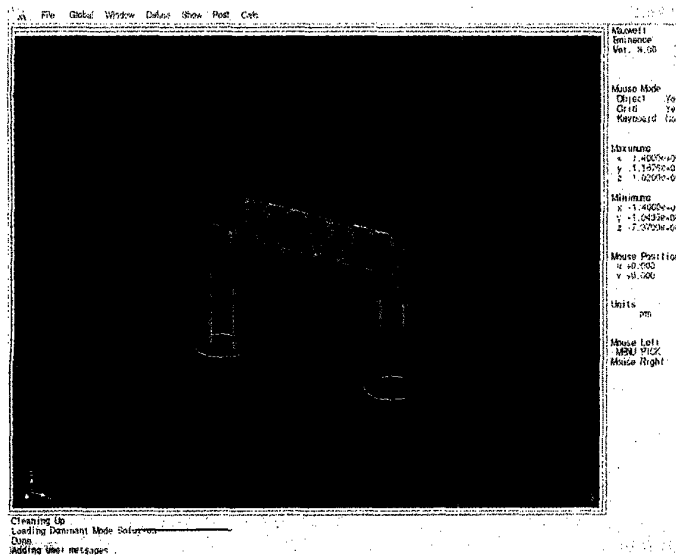


Figure 10b. The magnitude of the electric field at 6 GHz.

Figure 12a. A sinuous antenna with four coaxial feeds.

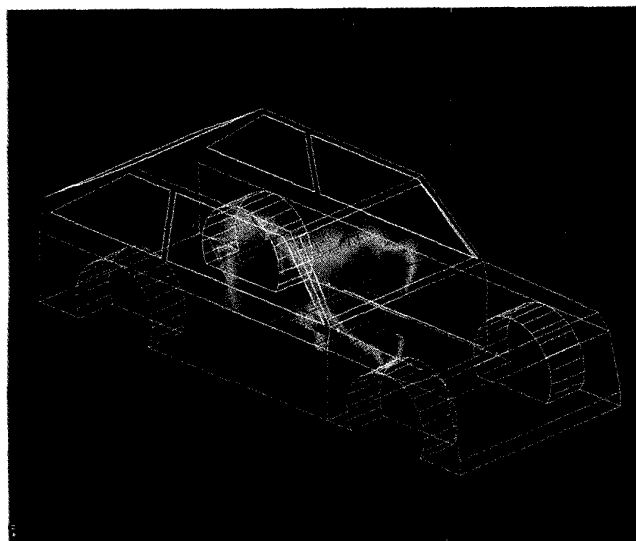
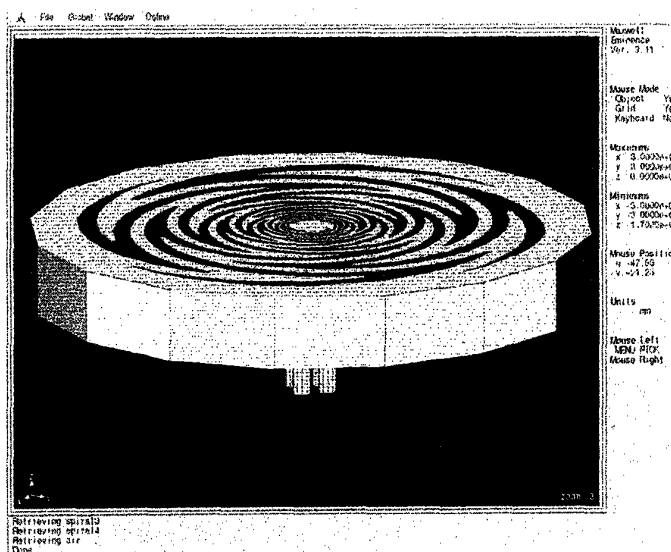


Figure 13. A simplified automobile model, showing emissions radiating from a data bus.

the frequency response over the entire bandwidth, from a single solution at a center frequency [44]. AWE determines this frequency response by computing the poles and residues of the transfer function for the linear system. Figure 9b presents a comparison of the computed s -parameters with measurements. The agreement is good over the entire frequency range, even though the finite-element solution was computed directly only at 10.5 GHz. The time required to obtain these results, including port solutions, mesh generation, and three adaptive-mesh-refinement passes was 20 minutes on an HP 735 computer.

Consider next the helix traveling-wave tube, shown in Figure 10a. This is a slow-wave structure, designed to allow an electron beam and an RF signal to interact. The helix geometry consists of eight ribbon-like turns, fed by two coaxial cables, and supported by three dielectric rods. The software predicts a phase velocity of 0.2128c for this structure, as well as a -47 dB return loss at 6.632 GHz. The magnitude of the electric field at 6 GHz is presented in Figure 10b.

Figure 11a shows one section of a phased-array antenna, consisting of many regularly spaced patch antennas. This antenna is excited by coaxial feeds, through the ground plane at the bottom, and is steered by varying the phase of the excitation. This antenna is solved in a similar way to that of the waveguide filter, except that the open region at the top was modeled as a multimoded waveguide containing 25 propagating modes. Changing the boundary conditions on these modes produces the effect of steering the beam.

Figure 11b shows the computed spectral response of the reflection coefficient at the input port for the antenna array, compared with measured values. A single solution at 2 GHz was used to extract ten poles in AWE to approximate the transfer function. The agreement is good in the range of measured values. The total solution time in this case was 40 minutes on an HP 735. It is interesting to note that a boundary-element code, specially designed to solve this problem, required more computer time to compute just one frequency point than was required by the general-purpose finite-element program to compute the entire broadband spectral response.

Figure 12a shows a sinuous antenna fed by four coaxial ports near the center of the structure. In this case, an absorbing-boundary condition (ABC) is used to truncate the finite-element solution, and to allow propagation into free space [45-49]. The far-field pattern is shown in Figure 12b, for both in-phase and out-of-phase excitations on ports 1 and 2. In these solutions, ports 3 and 4 where not excited. The agreement with measured results is good.

Finally, consider the problem of determining the electromagnetic compatibility of a data bus in an automobile. The data bus runs along the lower left side of the interior, and carries a 100 MHz. signal. Figure 13 shows a simplified automobile model, as well as the near-field and radiated emissions. The simulation provides details of these fields, including the effects of the front seat, dash, fire wall, and glass windows.

9. Conclusions

Finite-element methods present a much richer theory than was at first supposed. We now know that scalar finite elements are not sufficient to solve all electromagnetic-field problems. Spurious modes arise in the solution of the vector wave equation, if the wrong differential form is used to approximate the electric-field vector. Approximations of the electric field in the vector wave

equation must be done using tangential-vector finite elements, in order to avoid inconsistencies in the solution process.

Our present-day understanding of the causes of spurious modes in finite-element methods allows us to eliminate the problem. With reliability and robustness assured, computer programs that solve the vector wave equation by finite-element methods are proliferating. Programs such as *HFSS* and *Maxwell Eminence* set the standard for solving three-dimensional microwave problems, and break new ground in modeling complex-antenna and EMC problems. The examples presented here show the power of the finite-element method in solving problems containing difficult geometries and material properties. Thus, the promise of solving Maxwell's equations by finite-element methods, hinted at by Silvester's paper two-and-one-half decades ago, has finally come to fruition.

10. Appendix A.

High-Order Tangential Elements in Three Dimensions

In three dimensions, we approximate the electric field in terms of functions \mathbf{E}_e that interpolate to the tangential components of the field along the edges of a tetrahedron; \mathbf{E}_f that interpolate to the tangential components of the field on the faces of the tetrahedron; and \mathbf{E}_v that are associated with the normal components on the faces:

$$\mathbf{E} = \mathbf{E}_e + \mathbf{E}_f + \mathbf{E}_v. \quad (\text{A1})$$

The expression for \mathbf{E}_e is identical to Equation (27), except that the first summation is carried out over the six tetrahedron edges, instead of the three triangle edges. Similarly, \mathbf{E}_f is the same as Equation (34), except that the expression on the right-hand side is summed over the four tetrahedron faces, instead of having a value on just a single triangle face. The expression for \mathbf{E}_v is

$$\begin{aligned} \mathbf{E}_v = & \zeta_2 \zeta_3 \zeta_4 P^{(p-2)}(\zeta_2, \zeta_3, \zeta_4) \nabla \zeta_1 \\ & + \zeta_3 \zeta_4 \zeta_1 Q^{(p-2)}(\zeta_3, \zeta_4, \zeta_1) \nabla \zeta_2 \\ & + \zeta_4 \zeta_1 \zeta_2 R^{(p-2)}(\zeta_4, \zeta_1, \zeta_2) \nabla \zeta_3 \end{aligned} \quad (\text{A2})$$

\mathbf{E}_v is added only if $p > 1$. Here, $P^{(p-2)}(\zeta_2, \zeta_3, \zeta_4)$, $Q^{(p-2)}(\zeta_3, \zeta_4, \zeta_1)$, and $R^{(p-2)}(\zeta_4, \zeta_1, \zeta_2)$ are polynomials of degree $(p-2)$ in three dimensions. The total number of variables in \mathbf{E} is $(p+1)(p+3)(p+4)/2$.

11. References

1. A. Konrad, "Vector Variational Formulation of Electromagnetic Fields in Anisotropic Media," *IEEE Transactions on Microwave Theory and Techniques*, **MTT-24**, 1976, pp. 553-559.
2. M. Hara, T. Wada, T. Fukasawa, and F. Kikuchi, "Three-Dimensional Analysis of RF Electromagnetic Field by the Finite-element method," *IEEE Transactions on Magnetics*, **MAG-19**, 1983, pp. 2417-2420.
3. J. R. Winkler and J. B. Davies, "Elimination of Spurious Modes in Finite Element Analysis," *Journal of Computational Physics*, **56**, 1984, pp. 1-14.

4. K. Paulsen and D. Lynch, "Elimination of Vector Parasites in Finite Element Maxwell Solutions," *IEEE Transactions on Microwave Theory and Techniques*, **MTT-39**, March, 1991.
5. P. P. Silvester and G. Pelosi (eds.), *Finite Elements for Wave Problems*, New York, IEEE Press, 1994.
6. M. Hano, "Finite-Element Analysis of Dielectric-Loaded Waveguides," *IEEE Transactions on Microwave Theory and Techniques*, **MTT-32**, 1984, pp. 1275-1279.
7. S. H. Wong and Z. J. Cendes, "Combined Finite Element-Modal Solution of Three-Dimensional Eddy Current Problems," *IEEE Transactions on Magnetics*, **MAG-24**, 1988, pp. 2685-2687.
8. S. H. Wong and Z. J. Cendes, "Numerically Stable Finite-element Methods for the Galerkin Solution of Eddy Current Problems," *IEEE Transactions on Magnetics*, **MAG-25**, 1989, pp. 3019-3021.
9. C. W. Crowley, P. P. Silvester, and H. Hurwitz, "Covariant Projection Elements for 3D Vector Field Problems," *IEEE Transactions on Magnetics*, **MAG-24**, 1988, pp. 397-400.
10. A. Bossavit and I. Mayergoyz, "Edge-Elements for Scattering Problems," *IEEE Transactions on Magnetics*, **MAG-25**, 1989, pp. 2816-2821.
11. Z. J. Cendes, "Overview of CAE/CAD/AI Electromagnetic Field Computation," in A. Konrad (ed.), *Proceedings of the Second IEEE Conference on Electromagnetic Field Computation*, Schenectady, NY, 1987.
12. J. F. Lee, D. K. Sun, and Z. J. Cendes, "Tangential Vector Finite Elements for Electromagnetic Field Computation," *IEEE Transactions on Magnetics*, **MAG-27**, 1991, pp. 4032-4035.
13. A. F. Peterson, "Vector Finite Element Formulation for Scattering from Two-Dimensional Heterogeneous Bodies," *IEEE Transactions on Antennas and Propagation*, **AP-43**, 3, 1994, pp. 357-365.
14. Z. J. Cendes, D. Hudak, J. F. Lee, and D. K. Sun, *Development of New Methods for Predicting the Bistatic Electromagnetic Scattering from Absorbing Shapes*, RADC Final Report, Hanscom Air Force Base, MA, April, 1986.
15. Z. J. Cendes, "Vector Finite Elements for Electromagnetic Field Computation," *IEEE Transactions on Magnetics*, **MAG-27**, 1991, pp. 3953-3966.
16. P. Silvester, "Finite Element Solution of Homogeneous Waveguide Problems," *Alta Frequenza*, **38**, 1969, pp. 313-317.
17. Z. J. Cendes and P. Silvester, "Numerical Solution of Dielectric Loaded Waveguides. I - Finite-Element Analysis," *IEEE Transactions on Microwave Theory and Techniques*, **MTT-18**, 1971, pp. 1124-1131.
18. S. Ahmed and P. Daly, "Finite-Element Methods for Inhomogeneous Waveguides," *IEE Proceedings*, **116**, 1969, pp. 1661-1664.
19. A. Konrad, "Triangular Finite Elements for Vector Fields in Electromagnetics," PhD Thesis, Department of Electrical Engineering, McGill University, 1974.
20. Z. J. Cendes and S. H. Wong, "C1 Quadratic Interpolation Over Arbitrary Point Sets," *IEEE Computer Graphics and Applications*, November 1987, pp. 8-15.
21. D. Lynch and K. Paulsen, "Origin of Vector Parasites in Numerical Maxwell Solutions," *IEEE Transactions on Microwave Theory and Techniques*, **MTT-39**, March, 1991.
22. X. Yuan, D. R. Lynch, and K. Paulsen, "Importance of Normal Field Continuity in Inhomogeneous Scattering Calculations," *IEEE Transactions on Microwave Theory and Techniques*, **MTT-39**, 4, 1991, pp. 638-641.
23. J. P. Webb, G. L. Maile, and R. L. Ferrari, "Finite-Element Solution of Three-Dimensional Electromagnetic Problems," *IEE Proceedings*, **130**, Pt. H, 2, 1983, pp. 153-159.
24. S. M. Rao, D. R. Wilton, and A. W. Glisson, "Electromagnetic Scattering by Surfaces of Arbitrary Shape," *IEEE Transactions on Antennas and Propagation*, **AP-30**, 1982, pp. 409-418.
25. S. Wandzura, "Electric Current Basis Functions for Curved Surfaces," *Electromagnetics*, **12**, 1992, pp. 77-91.
26. A. Bossavit, "Whitney Forms: A Class of Finite Elements for Three-Dimensional Computations in Electromagnetism," *IEE Proceedings*, **135**, Pt. A, 8, 1988, pp. 493-500.
27. R. Albanese and G. Rubinacci, "Magnetostatic Field Computations in Terms of Two-Component Vector Potentials," *International Journal for Numerical Methods in Engineering*, **29**, March 1990, pp. 515-532.
28. J. Webb, "Edge Elements and what they can do for you," *IEEE Transactions on Magnetics*, **MAG-29**, 1993, pp. 1460-65.
29. J. P. Webb and B. Forghani, "A Single Scalar Potential Method for 3D Magnetostatics Using Edge Elements," *IEEE Transactions on Magnetics*, **MAG-25**, 1989, pp. 4126-4128.
30. J. P. Webb and B. Forghani, "The Low-Frequency Performance of H- ϕ and T- Ω Methods using Edge Elements for 3D Eddy Current Problems," *IEEE Transactions on Magnetics*, **MAG-29**, 1993, pp. 2461-2463.
31. P. Dular, A. Nicolet, A. Genon, and W. Legros, "A Discrete Sequence Associated with Mixed Finite Elements and its Gauge Condition for Vector Potentials," *IEEE Transactions on Magnetics*, **MAG-31**, 1995, pp. 1356-1359.
32. I. Bardi, O. Biro, K. Preis, G. Vrsk, K. Richter, "Nodal and Edge Element Analysis of Inhomogeneously Loaded 3D Cavities," *IEEE Transactions on Magnetics*, **MAG-28**, 1992, pp. 1142-1145.
33. J. B. Manges and Z. J. Cendes, "A Generalized Tree-Cotree Gauge for Magnetic Field Computation," *IEEE Transactions on Magnetics*, **MAG-31**, May 1995, pp. 1342-1347.
34. J. C. Nedelec, "Mixed Elements in R3," *Numer. Math.*, **35**, 1980, pp. 315-341.
35. *HFSS User's Manual*, Hewlett-Packard Company, Palo Alto, CA, 1990.
36. Z. J. Cendes, D. N. Shenton, and H. Shanassar, "Magnetic Field Computation Using Delaunay Triangulation and Complementary

Finite-element methods," *IEEE Transactions on Magnetics*, **MAG-19**, 6, November 1983, pp. 2551-2554.

37. D. N. Shenton and Z. J. Cendes, "Three-Dimensional Finite Element Mesh Generation Using Delaunay Tessellation," *IEEE Transactions on Magnetics*, **MAG-21**, 1985, pp. 2535-2538.

38. *Maxwell SI Eminence Users' Manual*, Ansoft Corporation, Pittsburgh, PA, 1994.

39. J. L. Yao Bi, L. Nicolas, and A. Nicolas, "H(curl) Elements on Hexahedral and Vector ABC's for Unbounded Microwave Problems," *IEEE Transactions on Magnetics*, **MAG-31**, May 1995, pp. 1538-1531.

40. T. V. Yioultsis and T. D. Tsiboukis, "Vector Finite Element Analysis of Waveguide Discontinuities Involving Anisotropic Media," *IEEE Transactions on Magnetics*, **MAG-31**, May 1995, pp. 1550-1553.

41. A. Ahagon and T. Kashimoto, "Three-Dimensional Electromagnetic Wave Analysis using High Order Edge Elements," *IEEE Transactions on Magnetics*, **MAG-31**, May 1995, pp. 1753-1756.

42. J. F. Lee, D. K. Sun and Z. J. Cendes, "Full-Wave Analysis of Dielectric Waveguides using Tangential Vector Finite Elements," *IEEE Transactions on Microwave Theory and Techniques*, **MTT-39**, 8, 1991, pp. 1262-1271.

43. Z. J. Cendes and J. F. Lee, "The Transfinite-element Method for Modeling MMIC Devices," *IEEE Transactions on Microwave Theory and Techniques*, **MTT-36**, 12, 1988, pp. 1639-1649.

44. X. Yuan, D. K. Sun and Z. J. Cendes, "AWEFEM: A Fast Method for Computing the Spectral Response of Microwave Devices over a Broad Bandwidth," *IEEE Transactions on Microwave Theory and Techniques*, submitted.

45. A. F. Peterson, "Absorbing Boundary Conditions for the Vector Wave Equation," *Microwave and Guided Wave Letters*, **1**, 2, April 1988.

46. J. P. Webb and V. N. Kanellopoulos, "Absorbing Boundary Conditions for the Finite Element Solution of the Vector Wave Equation," *Microwave and Guided Wave Letters*, **2**, 10, October 1989.

47. Y. Li and Z. J. Cendes, "High-Accuracy Absorbing Boundary Conditions," *IEEE Transactions on Magnetics*, **MAG-31**, May 1995, pp. 1524-1529. (48)

=====

President's Message Continued from page 6

Manufacturing Society (CPMT), Electron Devices Society (ED), Laser and Electro-Optics Society (LEO), Solid-State Circuits Council (SSC);

Division II - Industrial Applications

Dielectric and Electrical Insulation Society (DEI), Industry Applications Society (IA), Instrumentation and Measurement Society (IM), Power Electronics Society (PEL);

Division III - Communications Technology

Communications Society (COMM)

Division IV - Electromagnetics and Radiation

Antennas and Propagation Society (AP), Broadcast Technology Society (BT), Consumer Electronics Society (CE), Electromagnetic Compatibility Society (EMC), Magnetics Society (MAG), Microwave Theory and Techniques Society (MTT), Nuclear and Plasma Sciences Society (NPS);

Division V - Computers

Computer Society (COMP)

Division VI - Engineering and Human Environment

Education Society (Ed), Engineering Management Society (EM), Professional Communication Society (PC), Reliability Society (R), Society on Social Implications of Technology (SIT);

Division VII Energy and Power Engineering

Power Engineering Society (PE)

Division VIII - Computer

Computer Society (COMP)

Division IX - Signals and Applications

Aerospace and Electronics Systems Society (AES), Geoscience and Remote Sensing Society (GRS), Oceanic Engineering Society (OE), Ultrasonics, Ferroelectrics and Frequency Control Society (UFFC), Vehicular Technology Society (VT);

Division X - Systems and Control

Control Systems Society (CS), Engineering in Medicine and Biology Society (EMB), Industrial Electronics Society (IE), Information Theory Society (IT), Robotics and Automation Society Systems (RA), Man and Cybernetics Society, Neural Networks Council (NN).

One typically belongs to one or more of the above Divisions and Societies. All Antennas and Propagation Society members belong to **Division IV**. You should be able to identify your Division (or Divisions) and Society (or Societies). Additionally, Sections/Councils have local *Chapters*, based on technical areas of interests of the local professionals. On many occasions, several Societies form a joint Chapter, to cover the broad interest of local members. Again, the complete list of Chapters is too voluminous to be presented here. You should be able to get this information from your local Section/Council officials.

Note that you choose the Society (Societies) membership of your interest, whereas you are assigned a Region, depending on where you live. Clearly, each Chapter has its Chair, each Society has its Society President, each Division has its Division Director, each Section/Council has its Section/Council Chair, and each Region has its Region Director. You must identify who these people are, in order to establish an effective communication link. It is vitally important that you share your observations with these people. It is my hope that these officials will bring your suggestions and concerns to the attention of the right people for improving our organizational activities, in the vision of better serving the members. Remember that you deserve the best services possible, because without your financial, volunteer, and professional support, there will be no IEEE! Your input should count!

Please let me know if you have any problems in filling out the blank form for yourself. You may want to duplicate this form for each of your Society memberships. I envision that, one day, the IEEE will create a similar form, and distribute it to the new and existing members during the membership-subscription renewal. If

Continued on page 43